How to cite: *Angew. Chem. Int. Ed.* **2023,** *62,* e202217233
International Edition: doi.org/10.1002/anie.202217233
German Edition: doi.org/10.1002/ange.202217233

Metals in Medicine

Oral Anticancer Heterobimetallic Pt^{IV}–Au^{I} Complexes Show High In Vivo Activity and Low Toxicity

Tomer Babu, Hiba Ghareeb, Uttara Basu, Hemma Schueffl, Sarah Theiner, Petra Heffeter, Gunda Koellensperger,* Norman Metanis,* Valentina Gandin,* Ingo Ott,* Claudia Schmidt,* and Dan Gibson**

Abstract: Au^{I}-carbene and Pt^{IV}–Au^{I}-carbene prodrugs display low to sub-μM activity against several cancer cell lines and overcome cisplatin (cisPt) resistance. Linking a cisPt-derived Pt^{IV}(phenylbutyrate) complex to a Au^{I}-phenylimidazolylidene complex **2**, yielded the most potent prodrug. While in vivo tests against Lewis Lung Carcinoma showed that the prodrug Pt^{IV}(phenylbutyrate)-Au^{I}-carbene (**7**) and the 1:1:1 co-administration of cisPt: phenylbutyrate:**2** efficiently inhibited tumor growth (≈95 %), much better than **2** (75 %) or cisPt (84 %), **7** exhibited only 5 % body weight loss compared to 14 % for **2**, 20 % for cisPt and >30 % for the co-administration. **7** was much more efficient than **2** at inhibiting TrxR activity in the isolated enzyme, in cells and in the tumor, even though it was much less efficient than **2** at binding to selenocysteine peptides modeling the active site of TrxR. Organ distribution and laser-ablation (LA)-ICP-TOFMS imaging suggest that **7** arrives intact at the tumor and is activated there.

Introduction

Although chemotherapeutic agents are effective, they are often accompanied by severe side effects that are dose-limiting and hampered by developing drug resistance.[1] Therefore, clinicians treat patients with combinations of several drugs that differ from each other in their mode of action, cellular targets, and side effects.[2] Pt drugs are among the most widely used anticancer compounds (46 % of patients receive a Pt drug),[3] but not as single agents.[4] Different approaches can be applied to deliver several drugs to the tumor; the traditional way, where each drug is administered independently, encapsulating several drugs into a single carrier that unloads them in the tumor, or a single multi-action prodrug that upon cellular activation releases several drugs inside the cancer cell. Each approach has its pros and cons.[5]

The multi-action agent approach is dominant in the field of Pt anticancer agents primarily because inert octahedral Pt^{IV} complexes are exceptionally well suited to act as multi-purpose prodrugs that are activated by reduction inside the cancer cells, simultaneously releasing FDA-approved square planar Pt^{II} drugs [cisPt and oxaliplatin (oxaliPt)—Figure 1A and 1B] and up to two additional (bioactive) moieties in the axial positions (Figure 1C).[6] Pt^{II} complexes have been used worldwide for more than 50 years to treat cancer, mostly in combination with other anticancer drugs.[7] Their mechanism of action is based on the formation of intra-strand crosslinks preferentially between N7 of guanine DNA bases resulting in the induction of apoptosis.[8] They suffer from inherent or acquired resistance

[*] T. Babu, Dr. C. Schmidt, Prof. D. Gibson
Institute for Drug Research, School of Pharmacy, The Hebrew University of Jerusalem
Jerusalem 91120 (Israel)
E-mail: cla.schmidt@tum.de
dang@ekmd.huji.ac.il

H. Ghareeb, Prof. N. Metanis
Institute of Chemistry, The Center for Nanoscience and Nanotechnology, Casali Center for Applied Chemistry, The Hebrew University of Jerusalem
Jerusalem 9190401 (Israel)
E-mail: metanis@mail.huji.ac.il

Dr. U. Basu, Prof. I. Ott
Institute of Medicinal and Pharmaceutical Chemistry, Technische Universität Braunschweig
38106 Braunschweig (Germany)
E-mail: ingo.ott@tu-braunschweig.de

H. Schueffl, Prof. P. Heffeter, Prof. G. Koellensperger
Center for Cancer Research and Comprehensive Cancer Center (Austria)
E-mail: petra.heffeter@meduniwien.ac.at
gunda.koellensperger@univie.ac.at

Dr. S. Theiner
Institute of Analytical Chemistry, Faculty of Chemistry, University of Vienna
Waehringer Strasse 38, 1090 Vienna (Austria)

Prof. V. Gandin
Dipartimento di Scienze del Farmaco, Universita di Padova
35131 Padova (Italy)
E-mail: valentina.gandin@unipd.it

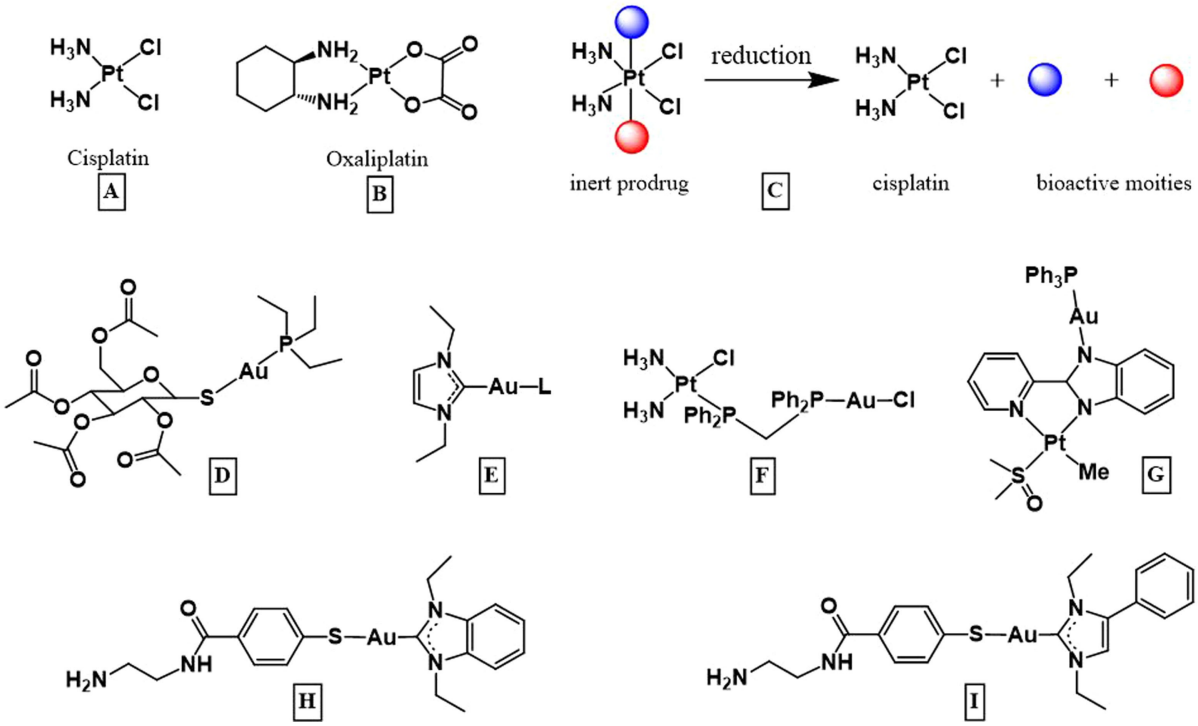

Figure 1. A) The FDA-approved Pt^{II}-based drugs, cisPt and B) oxaliPt, C) Pt^{IV} prodrugs that following cellular activation release cisPt and two axial ligands, D) Auranofin, E) General structure for Au–NHC complexes (L = thiols, phosphine, NHC etc.), F) Pt^{II}–Au^{I} conjugate linked by phosphines, G) Pt^{II}–Au^{I} conjugate that cannot form bifunctional lesions to DNA, H) EDA–MBA–Au–BeIm 1 and I) EDA–MBA–Au–PhIm 2.

as well as their dose-limiting side effects, such as nephrotoxicity, neurotoxicity, and ototoxicity. Their high reactivity towards extracellular nucleophiles results in low bioavailability and contributes to the side effects.[9] To overcome these shortcomings, multi-action Pt^{IV} prodrugs were studied with various bioactive axial ligands, primarily organic molecules.[6]

The bioactive axial moieties can also be non-platinum metal complexes, forming heterobimetallic prodrugs.[10] Particularly interesting are Au complexes derived from Auranofin (Figure 1D), an approved drug for the treatment of rheumatoid arthritis,[11] that is currently in clinical trial phase 1/2 for chronic lymphocytic leukemia (Identifier: NCT01419691)[12] and phase 1 trial for the treatment of recurrent epithelial ovarian, primary peritoneal,[13] and fallopian tube cancers (Identifier: NCT01747798).[13] Au^{I} complexes with *N*-heterocyclic carbene (NHCs) ligands (Figure 1E) are interesting anticancer agents as the NHC ligands stabilize the Au center and allow for a wide range of structural modifications and modulations at their backbone and wingtip positions.[14] Au complexes preferentially target thiol- or selenol-containing biomolecules and one of their most investigated and established cellular targets is the thioredoxin reductase (TrxR), a seleno-protein that is involved in the maintenance of the redox homeostasis and apoptosis.[15]

Combining a DNA-damaging Pt moiety and a TrxR-inhibiting Au^{I}-NHC scaffold can enhance anti-neoplastic activity, reduce side effects and overcome cisPt resistance. Heterobimetallic Pt^{II}–Au^{I} conjugates were previously reported but they are not true dual-targeting prodrugs that can simultaneously attack the DNA and TrxR. In one case, the Pt^{II} and Au^{I} were irreversibly bridged by phosphine linkers that prevent the detachment and separation of the metals (Figure 1F)[16] or the Pt^{II} moiety is unlikely to bind bifunctionally to DNA (Figure 1G).[17] In both cases, Pt binding to DNA was not reported. Heterobimetallic complexes of Au^{I} or Pt^{II} with Fe, Cu, Ru and Ti were recently reviewed.[18] Pt^{IV} heterobimetallic complexes were also described,[19] but to the best of our knowledge, there are no reports on heterobimetallic prodrugs that combine Pt^{IV} and Au^{I}.

Here, we combined in a single prodrug, the Pt^{IV} precursors of cisPt and oxaliPt with antiproliferative Au^{I}-NHC scaffolds bearing variations in the backbone position (Figure 1H and **I**) that were conjugated to the Pt^{IV} via an ethylenediamine-derivatized mercaptobenzoic (EDA-MBA) spacer.

Results and Discussion

Synthesis

Five heterobimetallic prodrugs and two novel Au^{I}-NHC complexes were prepared in this work (Figure 2). The synthesis is depicted in Scheme 1. These prodrugs were designed to attack two major cellular targets; nuclear DNA by cisPt/oxaliPt and TrxR by the Au–NHC and in complexes **4**, **5**, and **7** to also inhibit histone deacetylase (HDAC) and pyruvate dehydrogenase kinase (PDK) by phenylbutyrate (PhB). Based on previous work,[20] we chose

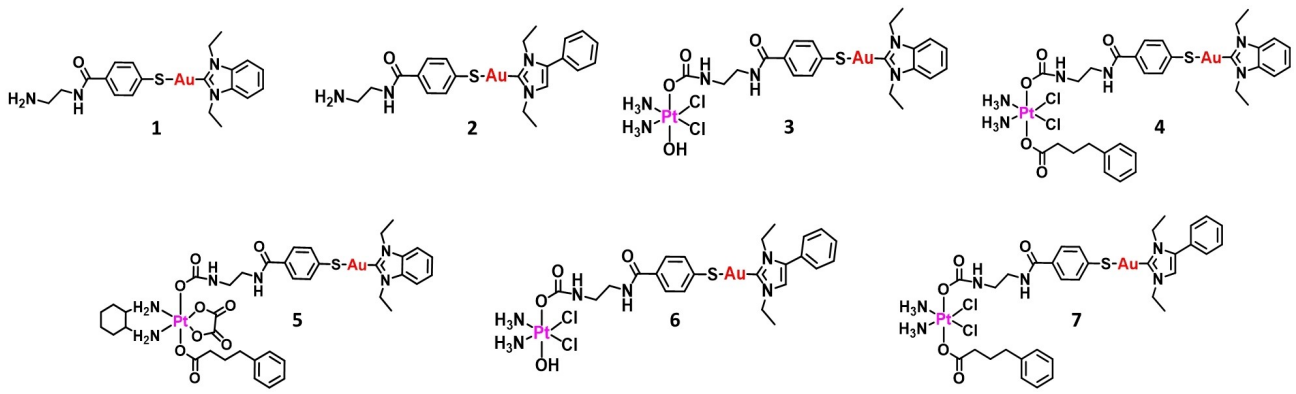

Figure 2. The NHC–Au–MBA-EDA complexes **1** (NHC = BeIm) and **2** (NHC = PhIm) and Pt^{IV}–Au^{I} complexes **3–7** used in this study.

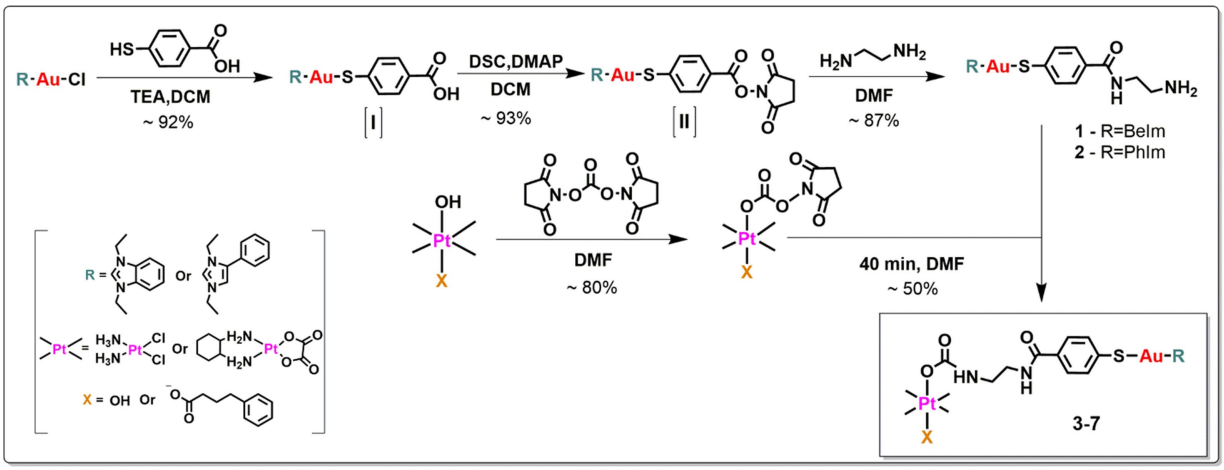

Scheme 1. Synthetic route for conjugating the Au^{I}–NHC to the Pt^{IV} via a carbamate linker.

the Au^{I}-NHC moiety as the TrxR inhibitor and MBA-EDA as the linker between the Au^{I} and the Pt^{IV}. Reduction of Pt^{IV} complexes with carbamate linkers results in rapid decarboxylation of the released axial ligands yielding molecules with a protonated primary amine, compounds **1** and **2**.

The synthesis, purification, and characterization details are described in the SI. All the final compounds were purified by HPLC, characterized by ^{195}Pt, ^{1}H, and ^{13}C NMR and ESI-MS and HPLC, and elemental analysis verified the purity. To our knowledge, this is the first report of a heterobimetallic Pt^{IV}–Au^{I} complex.

Table 1: The half-lives of the compounds in RPMI1640 medium and in the presence of ascorbic acid or GSH.

	Complex					
	2	**3**	**4**	**5**	**6**	**7**
$t_{1/2}$ RPMI1640 (h)	121	15.8	162	825	19	165
$t_{1/2}$ 10 equiv Asc (h)	–	1.2	10.9	70	0.9	11.2
$t_{1/2}$ 10 equiv GSH (h)	–	7.6	n.d	n.d	8.9	83
$t_{1/2}$ 20 equiv GSH (h)	–	7.2	n.d	n.d	8.4	78

n.d—not determined

Stability in Cell Culture Medium and Rates of Reduction

Pt^{IV} complexes are hypothesized to be stable outside the cell and reduced by biological reducing agents like ascorbic acid (Asc) and glutathione (GSH).[21] To verify this hypothesis, we monitored the stability of the compounds in cell culture medium and measured their rates of reduction in the presence of a tenfold excess Asc or GSH.

The half-lives in cell culture medium (RPMI1640/37 °C) and in excess Asc or GSH were measured by HPLC and are listed in Table 1. Prodrugs **4**, **5**, and **7** were very stable in cell culture medium with half-lives of 162, 825 and 165 h respectively. Prodrugs **3** and **6** were significantly less stable, with half-lives of 15.8 and 19 h, respectively. The differences in stability between the compounds can stem from the easier reduction of the former and/or from a protective steric effect of the PhB. The $t_{1/2}$ of **2** in 1 % DMSO and RPMI1640 medium was 121 h. The complexes with accessible equatorial chloridos and an axial hydroxido group (**3** and **6**) are more prone to reduction via a faster electron transfer from the Asc to the Pt^{IV} via an inner sphere mechanism. **5**, with the oxaliPt core, has only amine and carboxylate ligands and therefore, its reduction proceeds primarily by the slower outer sphere mechanism.[22]

This is evident in Table 1, where the half-lives for reduction of **3** and **6** by Asc are 1.4 and 0.9 h, respectively, significantly shorter than those for **4** and **7** with half-lives of 10.9 and 11.2 h, respectively. Carboxylation of the axial OH hinders the formation of an inner sphere bridge with the axial OH, and reduces the accessibility of the reducing agent to the equatorial chloridos due to the steric effect. **5** has the longest half-life (70 h). Asc, a two-electron reducing agent, reduces Pt^{IV} to Pt^{II} more efficiently than GSH, a one-electron donating agent,[23] even when the GSH concentration is double that of Asc (20 equiv. GSH vs. 10 equiv. Asc).

Characterization of the Reduction Products

We monitored the reduction of **4** in the presence of 10 equiv. of Asc at 37 °C in pH 7 by HPLC and confirmed the identity of the released ligands both by HPLC and MS analysis (Figure 3). **4** has a retention time of 5.80 min, while the free PhB ligand elutes at 4.99 min and **1** at 4.83 min. After 12 h of reaction with Asc ($\approx t_{1/2}$ of **4**), two new peaks appeared in the HPLC chromatogram with the same retention times as the free ligands. These assignments were confirmed by MS (Figure 3), indicating that decarboxylation of the carbamate occurred following the reduction, while the amide bond between EDA and MBA remains intact.

Antiproliferative Effects in Cancer and Non-Tumorigenic Cells

The antiproliferative effects of **3**–**6** were determined in a panel of cancer cell lines and non-tumorigenic kidney cells and compared to Auranofin, cisPt, and oxaliPt. After 72 h of incubation, all tested complexes showed IC_{50} values in the low or sub-μM range towards the entire panel of cancer cells. The cytotoxicity of the Au^{I} compounds **1** and **2** is also reported (Table 2).

Both **1** and **2** have IC_{50} values in the low to sub-μM range. **2** is significantly more potent than **1** in all cancer cell lines having an average IC_{50} value against all six cancer cell lines of 1.3 μM vs 9 μM for **1** and 7.2 μM for cisPt. Both compounds overcome acquired resistance to cisPt in the ovarian cancer cell lines with RF values ($RF = IC_{50(A2780cis)}/IC_{50(A2780)}$) of 1.38 and 2.00 for **1** and **2**, respectively, compared to 11.40 for cisPt. Notably, the IC_{50} values for **2** against these two cell lines are 0.28 and 0.56 μM (4.4 and 25.2-fold more potent than cisPt), while those for **1** are significantly higher 7.03 and 9.73 μM. **2** has a cytotoxicity profile that is significantly better than both **1** and cisPt which are quite similar.

Conjugating the BeIm–Au^{I} scaffold via a carbamate to $cisPt(OH)_2$ or cisPt(PhB)(OH) to yield **3** and **4**, respectively, significantly enhances the potency compared to both **1** or cisPt, particularly in the ovarian cancer cell lines. **3** and **4** have average IC_{50} values of 2.57 and 0.8 μM compared to 9 μM for **1** and 6.28 μM for cisPt. **4** is 3-10-fold more potent than **1** against the non-ovarian cancer cell lines and 17–20 fold more potent against the ovarian cancer cells. Interestingly, **4** is 1.3–3 fold more potent than **3** against all cancer cell lines. The difference

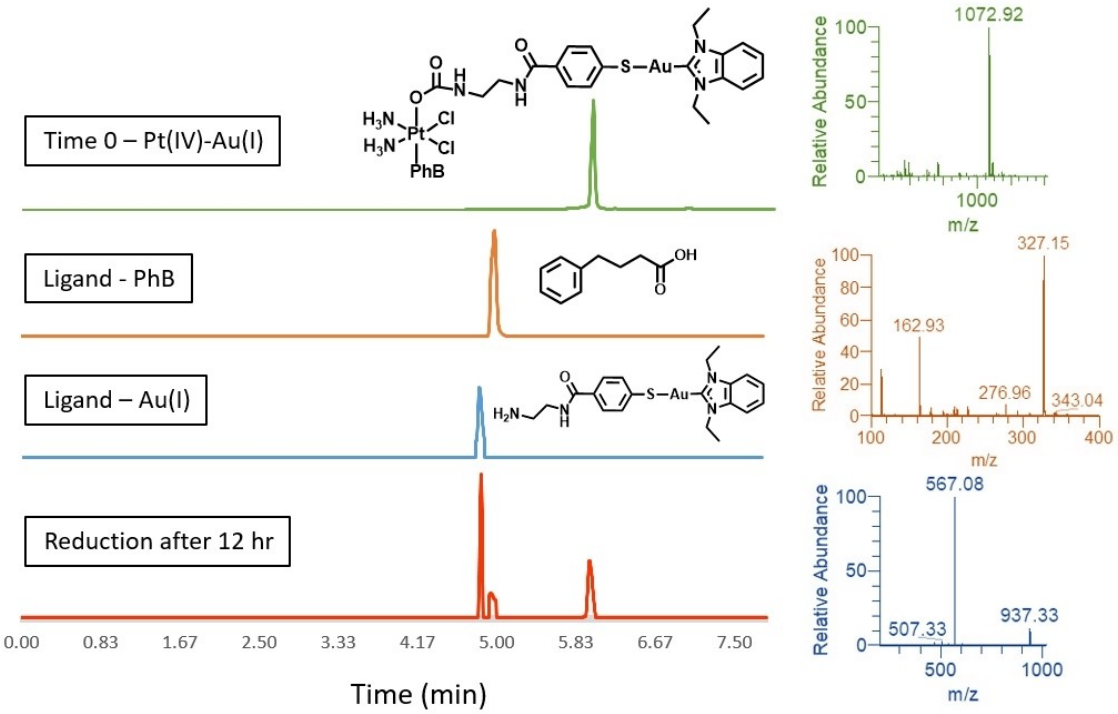

Figure 3. The HPLC chromatograms of **4** and the expected reduction products **1** and PhB together with their corresponding MS analyses (top 3 chromatograms) and a chromatogram of the reaction mixture following 12 h of incubation with 10 equiv of Asc (lower chromatogram).

Table 2: IC_{50} values [μM] after 72 h incubation (tested in triplicate).

Compound	A549 lung	HT-29 colon	MCF-7 breast	MDA-MB-231 breast	A2780 ovarian	A2780cis ovarian	VERO E6 healthy kidney
cisPt	3.39 ± 0.04	5.36 ± 0.19	11.27 ± 2.68	7.60 ± 0.40	1.24 ± 0.02	14.14 ± 0.12	8.58 ± 0.84
oxaliPt	1.00 ± 0.23	1.26 ± 0.18	0.76 ± 0.04	3.49 ± 0.45	0.34 ± 0.14	1.01 ± 0.17	0.79 ± 0.07
1	3.33 ± 0.18	11.52 ± 0.64	16.02 ± 4.36	6.35 ± 1.79	7.03 ± 0.05	9.73 ± 1.03	31.90 ± 2.12
2	0.57 ± 0.02	2.33 ± 0.17	2.87 ± 0.16	1.39 ± 0.33	0.28 ± 0.05	0.56 ± 0.16	22.89 ± 2.48
1/cisPt 1:1	3.19 ± 0.06	6.53 ± 0.08	12.01 ± 0.04	5.14 ± 1.24	1.07 ± 0.17	7.07 ± 0.001	9.58 ± 0.75
2/cisPt 1:1	0.38 ± 0.02	2.10 ± 0.11	2.54 ± 0.89	1.58 ± 0.47	0.15 ± 0.01	1.41 ± 0.01	17.85 ± 2.21
3	1.74 ± 0.97	4.30 ± 1.81	5.99 ± 0.89	2.27 ± 0.58	0.52 ± 0.13	0.65 ± 0.03	8.29 ± 1.00
4	0.41 ± 0.11	1.37 ± 0.11	1.63 ± 0.02	0.73 ± 0.18	0.41 ± 0.21	0.49 ± 0.17	9.20 ± 1.26
5	1.24 ± 0.30	3.44 ± 0.15	3.00 ± 0.97	1.77 ± 0.62	1.50 ± 0.36	3.11 ± 0.59	5.24 ± 0.33
6	0.85 ± 0.01	2.29 ± 0.23	2.34 ± 0.19	1.84 ± 0.34	0.16 ± 0.04	1.30 ± 0.03	8.73 ± 0.16
7	0.25 ± 0.01	0.97 ± 0.04	1.43 ± 0.29	0.99 ± 0.16	0.08 ± 0.001	0.15 ± 0.01	7.21 ± 0.40
Auranofin	3.84 ± 0.37	2.17 ± 0.45	1.39 ± 0.33	0.86 ± 0.08	–	–	2.96 ± 0.93

in activities between **3** and **4** might be attributed to the axial ligand of **4** (PhB) that increases lipophilicity and can inhibit HDAC activity.[24] Both **3** and **4** are more potent than cisPt and the 1:1 mixture of **1** and cisPt. The bimetallic Pt^{IV}–Au^{I}–complexes **3** and **4** are more active than the Au precursor or/and cisPt, and the Au scaffold is probably responsible for the ability to overcome cisPt resistance in ovarian cancer cells. Replacing the cisPt core of **4** with oxaliPt **5** resulted in a 2-fold to 6-fold reduction of activity.

The PhIm-containing Pt^{IV}–Au^{I} complex **6** had similar activity to **2** and the 1:1 mixture of **2** and cisPt (IC_{50} 0.16–2.34 μM for cancer cells and 8.73 μM for the VERO E6 cells), but was 2.3–10.9 times more active than cisPt alone. Again, the activity was enhanced by attaching the PhB ligand (**7**) resulting in an average IC_{50} of 0.65 μM for cancer cells and 7.21 μM for the non-cancerous cells.

To evaluate possible correlations between cytotoxicity and cellular uptake, we measured the Au and Pt content of A549 cells exposed to cisPt and to **1**, **2**, **4**, **6** and **7**. Compound **2** is 5.8-fold more potent than **1** (Table 2) and the uptake of the two Au compounds is quite similar and cannot explain the difference in potency (Figure S50). **7** and **4** display equal cellular accumulation and the former is 1.3-fold more potent. The 2.3-fold higher potency of **7** compared to **6** is greater than the difference in accumulation. Uptake is determined primarily by lipophilicity.

The selectivity indices ($SI = IC_{50}$ Vero E6/IC_{50} cancer cells) for **1** are 4.5 and 3.3 for A2780 and A2780cis, respectively. Interestingly, **2** is more selective towards the ovarian cancer cells compared to **1**, (SI = 81.8 and 40.9). Conjugating **1** to oxoplatin to yield **3**, significantly improved the selectivity indices (15.9 and 12.8). The PhB containing prodrugs exhibit selectivity indices of 54.6 and 6.7 for **6** and 90.1 and 48.0 for **7**. The selectivity indices values for the PhIm-based complexes are quite striking compared to the selectivity indices of cisPt, (6.9 and 0.6). The selectivity indices for **7** (A549) is ≈30, while the cellular accumulation in A549 is only 25 % higher than in Vero E6 (Figure S51) meaning accumulation plays a minor role in selectivity.

Extracellular and Intracellular Inhibition of Thioredoxin Reductase Activity

The inhibition assay of TrxR was performed with the isolated enzyme in a 5,5′-dithiobis-(2-nitrobenzoic acid (DTNB)-based assay, and the IC_{50} values were calculated after incubation for 75 min at 37 °C.

As controls, we used cisPt and oxaliPt, which were inactive ($IC_{50} > 50$ μM), as well as Auranofin (IC_{50} 93 nM). The Au complexes **1** and **2** have IC_{50} values in the low μM range (IC_{50} 2–3 μM), whereas all the heterobimetallic Pt^{IV}–Au^{I} conjugates have lower IC_{50} values (0.15–0.76 μM). **3**, **4**, and **5** were 6, 14 and 10-fold more potent compared to **1**, while **6** and **7** were 11 and 4-fold more potent than **2**. None of the test compounds outperformed Auranofin.

Interestingly, the inhibitory activity of **6** and **7** decreased when the complexes were pre-incubated for 24 h with an excess of Asc in phosphate buffer at 37 °C (Table 3), probably due to reduction of the complexes and release of **2**, which is significantly less potent than **6** or **7**.

We evaluated the ability of **7**, **2**, cisPt, and a 1:1 mixture of **2** and cisPt to inhibit TrxR activity in A549 cells, which

Table 3: Inhibition of the isolated TrxR at 37 °C for 75 min (solvent of stock solutions in brackets, if not further described DMF was used).

Compound	IC_{50} isolated TrxR [μM]	IC_{50} TrxR in A549 cells [μM]
cisPt (H_2O)	> 50	31.4 ± 2.6
oxaliPt (H_2O)	> 50	n.d.
1	2.088 ± 0.131	n.d.
2	3.027 ± 0.128	19.2 ± 0.1
3	0.373 ± 0.010	n.d.
4	0.151 ± 0.009	n.d.
5	0.202 ± 0.005	n.d.
6	0.283 ± 0.048	n.d.
7	0.755 ± 0.029	5.5 ± 0.6
6[a] + 10 equiv ascorbic acid	0.751 ± 0.077	n.d.
7[a] + 10 equiv ascorbic acid	1.668 ± 0.064	n.d.
2 (DMF) + cisPt (1:1)	3.270 ± 0.048	28.4 ± 1.9
Auranofin	0.093 ± 0.009[24]	0.30 ± 0.05

[a] preincubation for 24 h before adding TrxR, n.d. = not determined.

highly express TrxR.[25] Using a modified reported method,[26] we performed an end-point insulin reduction assay, where the number of thiol groups was determined spectrophotometrically using DTNB. To eliminate the effects of other cellular reductases, we used two sets of experimental conditions for each concentration of the test compounds; one having recombinant TrxR as the substrate and the other without it. The activity of the TrxR itself was obtained from the difference in the absorbance values between the two sets of experimental conditions, allowing us to obtain the specific cellular TrxR activity following 24 h of exposure to the compounds.

7 inhibits the enzyme at an IC_{50} of 5.5 μM, while **2** has IC_{50} values near 20 μM and cisPt 31.4 μM. Co-incubation of cisPt and **2** did not show any synergistic effects (IC_{50} 28.5 μM). Importantly, this order of activity (**7** ≫ **2** > cisPt) agrees with the results obtained against purified TrxR (Table 3).

7 is about 3.5-fold more efficient than **2** at inhibiting TrxR in A549 cells. While it is tempting to ascribe this to the somewhat higher accumulation of **7** (Figure S49), the inhibition studies against the isolated enzyme indicated that all the Pt–Au compounds **3**–**7** are superior TrxR inhibitors compared to **1** and **2**, implying that the higher effect of **7** is not due primarily to accumulation.

Comparing the IC_{50} values for cellular TrxR inhibition with those for cytotoxicity (Table 2) indicates that TrxR inhibition occurs at much higher concentrations than cytotoxicity. However, different assay conditions must be considered. For example, cytotoxicity is determined after 72 h of rapid cell proliferation, whereas TrxR activity is evaluated after 24 h of exposure to an almost confluent (not strongly proliferating) cell layer.

Reactivity of the Compounds Towards Cysteine- and Selenocysteine-Containing Peptides

A potential target for Au^I complexes is the TrxR family, that plays a significant role in the intracellular redox homeostasis. Seleno-enzymes (containing the rare 21st encoded amino acid selenocysteine (Sec, U) are possible targets for the development of new anticancer agents.[27] A strong inhibition of TrxR activity can lead to a change in the mitochondrial membrane potential which eventually may lead to apoptosis via the intrinsic pathway.[28] Au^I complexes, like Auranofin (Figure 1D), are potent and selective inhibitors of TrxR, due to interactions between the Au^I core and the selenium or sulfur. Messori et al. investigated their mechanism of inhibition by monitoring their binding to peptides that contain Sec and Cys by ESI-MS studies.[29]

We designed Pt^{IV}–Au^I prodrugs assuming that following reduction, the cationic EDA–MBA–Au–NHC moiety will efficiently inhibit TrxR. Surprisingly, the Pt–Au compounds **3**–**7** were significantly better TrxR inhibitors than the Au compounds **2** and **1**, both against isolated TrxR and against TrxR *in cellulo* (Table 3). We prepared 4 model peptides that contain either Sec, Cys, both or none (Figure 4A) and studied their interactions with **4**, **1** and **2**.

The model peptides (Figure 4A) were synthesized through SPPS procedure (SI). As shown in Figure 4A, the Sec-containing peptides (A and B) were isolated in the oxidized state. Thus, we tested the interactions of the peptides with the complexes in both the oxidized and reduced states. There was no significant reaction between compounds **1**, **2, 4** or **7** with the oxidized peptides A and B, nor with peptide D that lacks Cys or Sec or with C that has a reduced Cys.

The reduced peptides were obtained by adding 5 equiv. of dithiothreitol (DTT) at RT for 5 min and were then reacted with 1 equiv of the complexes for 30 min at 37 °C. We confirmed that **1**, **2, 4** and **7** were stable in the presence of DTT. Reactions were monitored by HPLC and the new peaks that formed were collected and characterized by MS. In all cases, either Au–NHC or just Au moieties were bound to the Sec residue suggesting that the Se displaced the thiolate (rather than the NHC) from the Au (Figure 4B). Both the *m*/*z* values and the isotopic patterns confirmed the identity of the conjugates (example in Figure 4C/D). This agrees with a previous report on the interaction of Au–NHCs, with seleno-peptides.[30]

While the reactions of peptide A with both **1** and **2** were completed after 30 min, only 15–20 % conversion was observed for the reactions with **4** and **7** (Figure 4B, S49). Yet, the same products were obtained, direct binding of the Au–NHC to the Sec residue. This is perplexing because **4** and **7** are much better TrxR inhibitors than compounds **1** and **2**.

As B contains both Sec and Cys, the reduction of the peptide exposed the two soft nucleophiles (Sec and Cys) capable of reacting with heavy metals. Both Au^I derivatives **1** and **2** were allowed to react for 30 min with the reduced peptide at 37 °C. As with A, complete conversion occurred within 30 min, yielding two main peaks corresponding to either peptide B–Au–NHC or peptide B–Au conjugates (Figure 4B). Once again, after 30 min of reaction between B and **4** or **7**, only 15–20 % conversion was observed with a single product (peptide B–Au–NHC).

Peptide B was designed to include an Arg residue before the Sec, and a Lys residue between the Sec and the Cys, making it contusive to trypsin digestion. The trypsin digest of the modified peptide B should give three fragments, one containing the Sec and another containing the Cys, allowing us, in principle, to establish the binding site of the Au. We performed trypsin digestion on an isolated peptide B–Au conjugate in a 1:30 ratio for 30 min at 37 °C. We isolated two products with *m*/*z* values that match the cleaved sequence of Ser–Glu–Phe–Gly–Arg and also His–Trp–Cys–Tyr–Lys; neither had Au bound to it. Unfortunately, we could not observe a product with *m*/*z* that contains Sec with or without Au (Figure S48). Nonetheless, based on the observation that the cysteine thiol in peptide C did not react with the Au compounds, we presume that the Au is bound solely to the Se in peptide B.

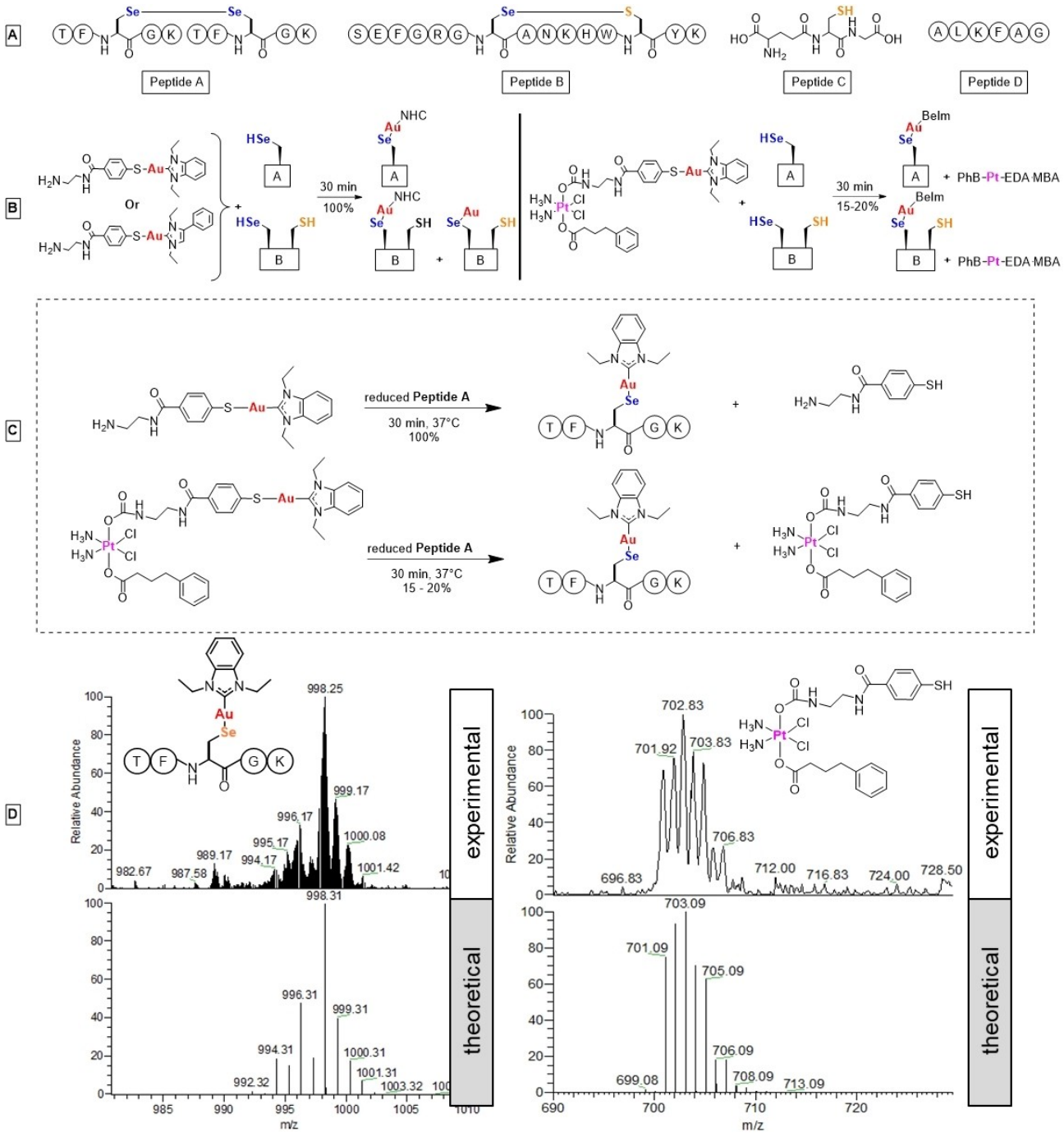

Figure 4. A) The peptides used in this study; B) Summary of the reactions between **1** and **4** with A and B; C) a more detailed description of the reaction between **4** and A; D) experimental (top) and simulated (bottom) ESI-MS for the reaction between **4** and A.

In Vivo Efficacy and Toxicity

We performed preliminary in vivo anticancer studies comparing cisPt, **2** and **7** against the murine Lewis Lung Carcinoma (LLC) solid tumor model. Cytotoxicity of the compounds was first assessed in LLC cells (Table S1). LLC is a highly aggressive and metastatic syngeneic carcinoma characterized by high reproducibility, and as allograft, it is performed in immune-competent mice. Using an immuno-competent animal model is crucial to understanding the great contribution of immunity/inflammation to cancer initiation and progression.[31]

Seven days after tumor inoculation, the tumor-bearing mice were randomized into vehicle control and treatment groups. Control mice received the vehicle [1 % DMSO (v/v) and 99 % of a saline solution (v/v)], whereas treated animals received every 2 days (days 8, 10, 12 and 14): oral gavage of 12 mg kg^{-1} of **7** or i.p. injections of 4 mg kg^{-1} of **2**, 4 mg kg^{-1}

of cisPt, 4 mg kg^{-1} of PhB and a combination of 4 mg kg^{-1} each of cisPt, **2** and PhB. On day 15, animals were sacrificed and the tumor weight was evaluated; the results are summarized in Table 4.

PhB did not inhibit tumor growth, while **2** induced a 75 % reduction of tumor mass, slightly lower than cisPt (84 %). The efficacy of **7** was significantly higher than that of cisPt or **2** (≈94 % tumor reduction). Interestingly, the combined administration of cisPt, **2** and PhB resulted in 96 % tumor inhibition, similar to **7** (94 %).

While both **7** and the combination therapy were effective at inhibiting tumor growth, there is a huge difference between them in acute toxicity as manifested by body weight loss (Figure 5). Animal body weights were monitored at day 0 and from day 7 onward every 2 days as a sign of systemic toxicity (Figure 5). The time course of body weight changes shows that treatment with **7** resulted in only a few percent weight loss. In contrast, treatment with cisPt or **2** resulted in a ≈20 % and 15 % loss, respectively. The combination of cisPt, **2**, and PhB induced a weight loss of nearly 30 %.

The preliminary in vivo efficacy results clearly demonstrate the advantage of using a Pt^{IV}–Au^{I} prodrug compared to the combination treatment, particularly regarding reduced systemic toxicity.

We assessed the inhibition of TrxR activity in the tumors of the treated animals. Tumors of control or treated animals were collected on day 15, weighed and homogenized. TrxR activity was assessed by the DTNB assay. Results reported in Figure 5 clearly confirm that PhB does not affect TrxR activity. CisPt induced only a minimal reduction of TrxR activity, whereas **2** induced a 30 % reduction of enzyme activity. Interestingly, both **7** and the combination treatment with cisPt, PhB and **2** reduced TrxR activity by 45 %. As in the TrxR inhibition studies against the isolated enzyme and the inhibition of the cellular activity of TrxR, **7** outperforms **2** as a TrxR inhibitor in vivo. This confirms that Pt^{IV}–Au^{I} prodrugs target TrxR in vivo.

We evaluated and compared the biodistribution and toxicity profiles for treatment with **7** and a combination of **2**, cisPt and PhB. Tumor homogenates employed for TrxR analysis as well as kidney, intestine, lung, and liver of treated animals were subsequently mineralized and the Au and Pt content of each sample was measured by ICP-MS (Figure 6). As expected, in the combination treatment there are large differences in the biodistribution of the Pt and Au. The Pt accumulates primarily in the kidney, while the Au accumulates preferentially in the liver. Interestingly, similar levels of Pt and Au accumulated in the tumor when treated with **7** or with the combination treatment, suggesting that effective tumor inhibition requires both the Pt and the Au. Notably, in the case of **7**, the Pt and Au levels in all the organs and in the tumor were very similar, suggesting that the prodrug is sufficiently stable for targeting the tumor site.

To gain a deeper understanding of the intratumoral distribution of **7** compared to the single treatment combining **2** and cisPt, multi-elemental analysis via laser-ablation (LA)-ICP-TOFMS was performed. Tumor-bearing mice were dosed once with cisPt + **2** (4 mg kg^{-1} each, i.p.) or **7** (12 mg kg^{-1}, oral gavage). After 5 h, the tumors were harvested, embedded in optimal cutting temperature compound (OCT), and cryo-sections were prepared. They were analyzed for the Pt, Au, and endogenous element distribution at the microscale using LA-ICP-TOFMS imaging (Figure 7A). Consecutive slices were stained with hematoxylin and eosin (H/E) (for visualization of the general tissue morphology) and the von Willebrand factor (for localization of micro blood vessels).[32] In general, slightly higher Pt and Au levels were observed in the combination-treated animals, which is not surprising as the i.p. route of drug administration results in 100 % bioavailability in contrast to p.o. administration. There were distinct differences in the intratumoral drug distribution patterns of the two treatments.

Table 4: In vivo tumor inhibition studies.

Compounds	Daily dose [mg kg^{-1}]	Average tumor weight (mean ± SD, gr)	Inhibition of tumor growth [%]
control	–	0.551 ± 0.10	–
cisPt	4	0.086 ± 0.04[a]	84.4
PhB	4	0.525 ± 0.06	4.7
2	4	0.138 ± 0.02[a]	74.9
cisPt + **2** + PhB	4 + 4 + 4	0.021 ± 0.02[a]	96.2
7	12	0.035 ± 0.01[a,b]	93.7

[a] $p < 0.05$ (respect to control); [b] $p < 0.1$ (respect to 2).

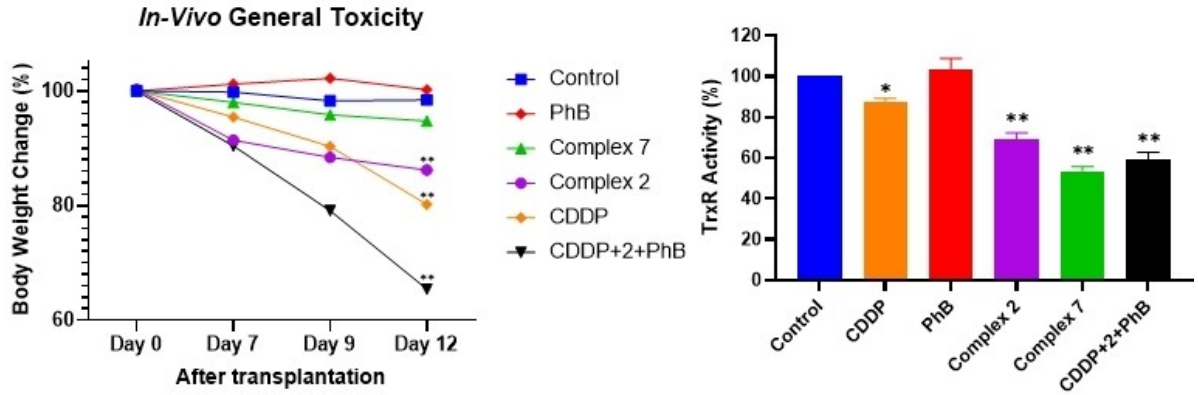

Figure 5. Body weight changes (left) and in vivo TrxR inhibition (right). A. Error bars indicate the S.D. $^{**}P < 0.01$; $^{*}P < 0.05$.

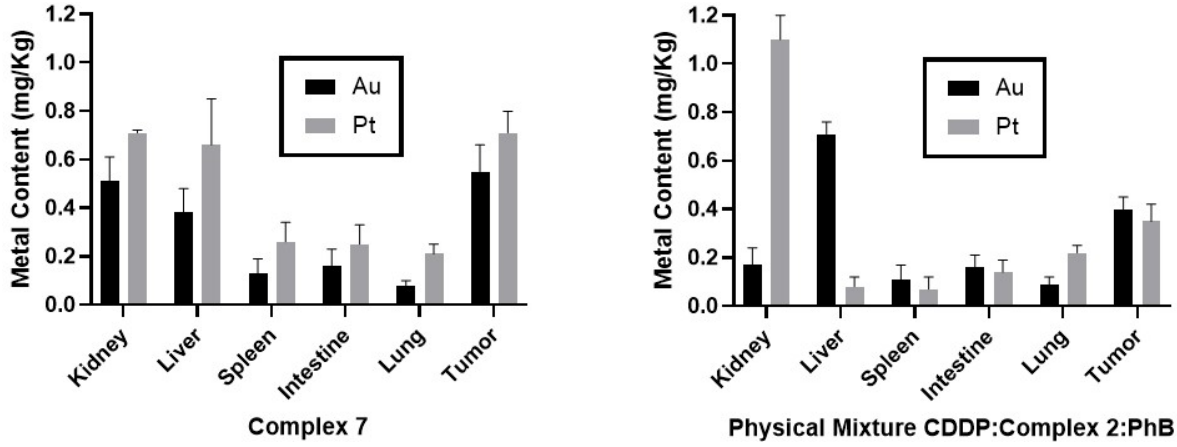

Figure 6. In vivo biodistribution profiles of **7** (left) and combination of cisPt:PhB:**2** (right) in LLC-bearing C57BL mice. Error bars indicate the S.D.

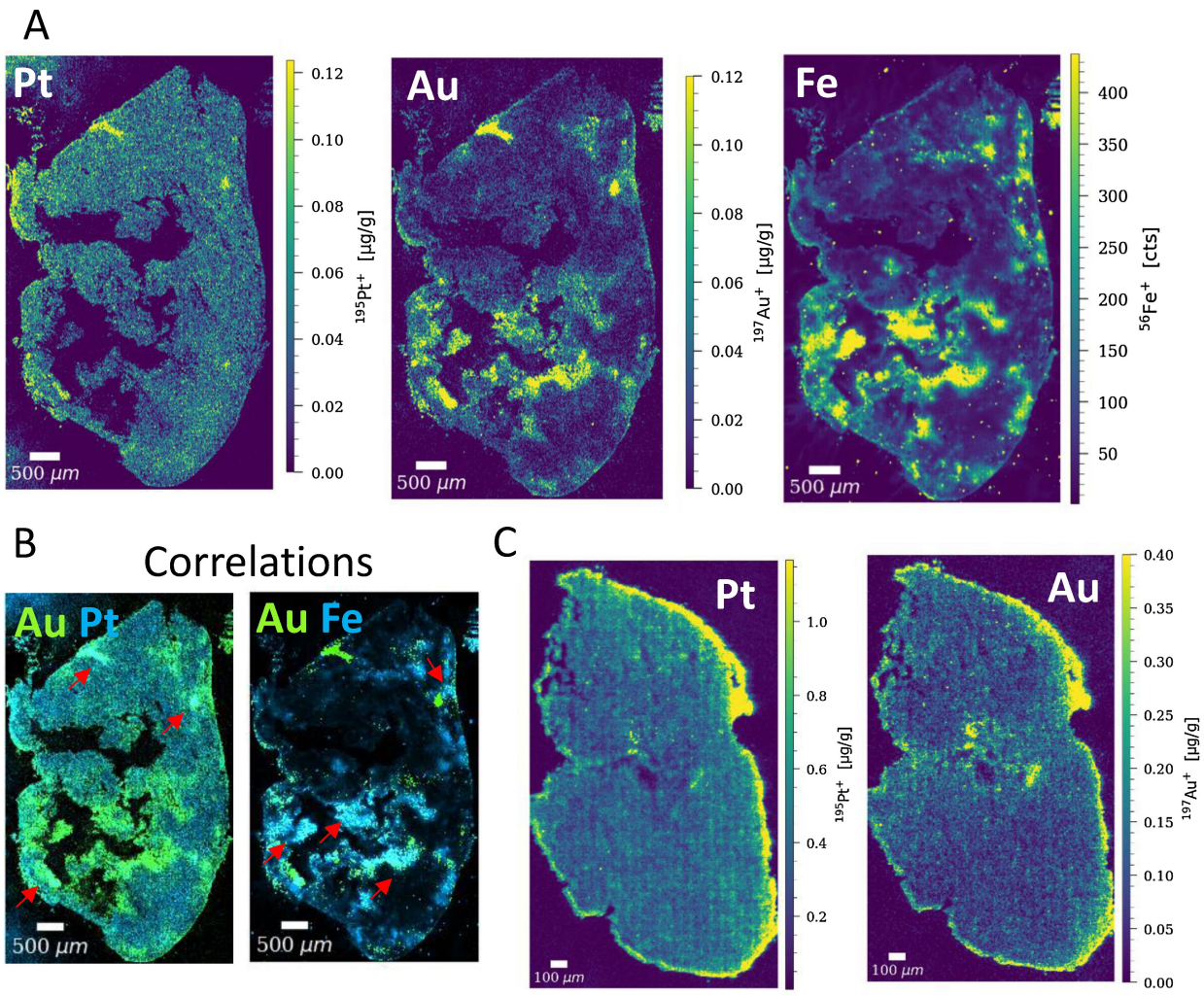

Figure 7. Intratumoral elemental distribution of cryo-sections via LA-TOFMS imaging of LLB-bearing C57BL mice after 5 h (A) one single treatment of prodrug **7** or (C) the single drug combination of **2** and cisPt. In (B) the correlations in the **7**-treated section of Au with either Pt or Fe are depicted (red arrows).

While a rather even Pt and Au distribution over the tumor tissue was observed for the drug combination (Figure 7C), in samples of **7**, several Pt and Au hotspots were visible in the tissue. Noteworthy, some of these hotspots (indicated by

arrows) showed a strong correlation between the Pt and Au signals, indicating that at these spots, the compound arrived intact at the tumor (Figure 7B). In several areas, Au co-localized with Fe hotspots. Histological examinations showed that these areas are high in blood vessel density thus, close to the entrance into the malignant tissue.

The colocalization of the Au and the Fe, in conjunction with the more even distribution of the Pt, suggests that the compound arrives intact at the tumor site, possibly carried by albumin, where the Pt^{IV} is reduced and the released cisPt diffuses deeper into the tissue, while the released Au binds to albumin.

Nephrotoxicity is the most common dose-limiting toxicity of Pt-based drugs, and is one of the major causes of discontinuing therapy.[33] Irreversible kidney damage occurs in about one-third of cisPt-treated patients. While, liver injury is a major setback induced by FDA-approved Au^I drugs.[34]

The potential nephrotoxic and hepatotoxic effects induced by treatment with **7**, **2**, cisPt, PhB or the combination cisPt: PhB:**2** were also evaluated by measuring some specific biomarkers. For kidney injury, the urines of control and treated mice were analyzed for urinary total protein (uTP) and *N*-acetyl-β-*D*-glucosaminidase (NAG) (Figure 8A). CisPt induced a significant increase of uTP excretion and NAG, whereas PhB did not alter either of those biomarkers. Although **7** elicited an increase in NAG activity, it was significantly lower compared with cisPt and the combination treatment.

The specific biomarkers alanine transaminase (ALT) and aspartate aminotransferase (AST) for liver injury as well as TrxR levels were measured in serum samples of control and untreated mice (Figure 8B and C). **2**, **7**, PhB and cisPt did not adversely affect liver function, whereas the combination treatment partially altered the serum levels of these biomarkers (Figure 8B). However, none were as toxic as CCl_4, a standard reference that dramatically increased biomarkers' levels. TrxR serum levels were not significantly altered by treatment with all tested compounds (Figure 8C).

These organ-specific toxicity results clearly demonstrate the advantages of **7** compared to the combination treatment in terms of significantly reduced nephro- and hepato toxicities, suggesting that even prodrugs containing two heavy metals can be safe and effective.

Conclusion

The two Au^I compounds **1** and **2** are quite potent cytotoxic agents with IC_{50} values in the low μM range with high selectivity to cancer cells. Potency depends on the nature of the NHC ligand. The PhIm complex **2** was significantly more potent than the BeIm complex **1** or cisPt in all cancer cell lines tested. The most potent Pt^{IV}–Au^I prodrugs **4** and **7** had an axial PhB ligand, that enhanced accumulation. The hypothesis was that the released Au^I-NHC moiety will effectively inhibit TrxR. Surprisingly, all the intact Pt^{IV}–Au^I prodrugs were significantly more potent inhibitors of TrxR compared to the Au compounds. Interestingly, this trend of activity (**7** ⩾ **2** > cisPt) was also observed in TrxR inhibition in cancer cells and in mice with LLC tumors. We studied the interactions of the most potent inhibitor **4** of isolated TrxR and the two Au^I compounds with peptides that model the TrxR-binding site for Au^I. Contrary to expectations, the weaker TrxR inhibitors **1** and **2** reacted significantly more efficiently with the Sec peptides than the much more potent inhibitor **4**. In aggregate, this suggests that inhibition of TrxR by the Pt^{IV}–Au^I compounds might involve other factors besides the direct binding of the Au^I to the selenocysteine.

We confirmed that the prodrug targets TrxR in vivo at the tumor site and hampers its activity, thereby contributing to the efficient inhibition of tumor growth. Moreover, in vivo studies clearly demonstrate the differences between the two pharmacological approaches: multi-targeting (one drug) and multiple targeting (several drugs). In particular, efficacy and toxicity studies allow us to highlight the toxicological advantages of utilizing a single small molecule that modulates multiple targets compared to combinations of multiple drugs.

Heavy metals such as Pt and Au are expected to have severe toxicities. Yet, the Pt^{IV}–Au^I multi-targeting prodrug is as efficacious as the combination treatment in vivo but, importantly, is significantly less toxic than either cisPt or the combination treatment, demonstrating the advantages of the multi-targeting strategy to pursue smart medicines for anticancer chemotherapy further.

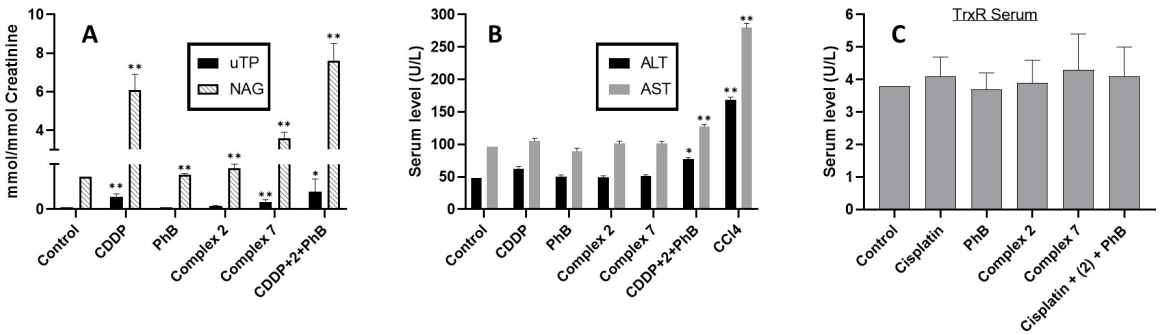

Figure 8. In vivo nephrotoxicity (A) and hepatotoxicity (B) profiles as well as serum TrxR levels (C). Urines (A) and sera (B + C) of control and treated mice were subjected to biomarkers detection by ELISA assays. Error bars indicate the S.D. $^{**}P < 0.01$; $^{*}P < 0.05$.

Acknowledgements

D.G. and N.M. acknowledge support from the Israel Science Foundation (1002/18, and 1388/22, respectively). T.B. thanks Clore Israel Foundation for scholar Ph.D. fellowship. The author H.G. thanks the British Council for GROWTH Ph.D. Fellowship. P.H. and G.K. acknowledge the financial support from the FG3 Forschungsgruppe (FWF) and from the City of Vienna Fund for Innovative Interdisciplinary Cancer Research (Project No. 21206).

Conflict of Interest

The authors declare no conflict of interest.

Data Availability Statement

The data that support the findings of this study are available from the corresponding author upon reasonable request.

Keywords: Au^{I}-Carbene · Heterbimetallic · Multi-Targeting · Prodrugs · Pt^{IV}

[1] a) K. Hauner, P. Maisch, M. Retz, *Urologe* **2017**, *56*, 472–479; b) K. Bukowski, M. Kciuk, R. Kontek, *Int. J. Mol. Sci.* **2020**, *21*, 3233.
[2] a) G. Garcia, M. Odaimi, *J. Gastrointest. Cancer* **2017**, *48*, 121–128; b) T. Boulikas, M. Vougiouka, *Oncol. Rep.* **2004**, *11*, 559–595.
[3] E. Armstrong-Gordon, D. Gnjidic, A. J. McLachlan, B. Hosseini, A. Grant, P. J. Beale, N. J. Wheate, *J. Cancer Res. Clin. Oncol.* **2018**, *144*, 1561–1568.
[4] I. S. Um, E. Armstrong-Gordon, Y. E. Moussa, D. Gnjidic, N. J. Wheate, *Inorg. Chim. Acta* **2019**, *492*, 177–181.
[5] a) Z. G. Wang, Z. Q. Deng, G. Y. Zhu, *Dalton Trans.* **2019**, *48*, 2536–2544; b) K. K. Jain, *Methods Mol. Biol.* **2014**, *1141*, 1–56.
[6] a) D. Gibson, *Dalton Trans.* **2016**, *45*, 12983–12991; b) M. Ravera, E. Gabano, M. J. McGlinchey, D. Osella, *Inorg. Chim. Acta* **2019**, *492*, 32–47; c) R. G. Kenny, C. J. Marmion, *Chem. Rev.* **2019**, *119*, 1058–1137.
[7] S. Alassadi, M. J. Pisani, N. J. Wheate, *Dalton Trans.* **2022**, *51*, 10835–10846.
[8] S. Dasari, P. B. Tchounwou, *Eur. J. Pharmacol.* **2014**, *740*, 364–378.
[9] R. Oun, Y. E. Moussa, N. J. Wheate, *Dalton Trans.* **2018**, *47*, 6645–6653.
[10] N. Curado, M. Contel, *RSC Metallobiol.* **2019**, *14*, 143–168.
[11] a) C. F. Shaw, *Chem. Rev.* **1999**, *99*, 2589–2600; b) H. Ghareeb, N. Metanis, *Chem. Eur. J.* **2020**, *26*, 10175–10184.
[12] https://clinicaltrials.gov/ct2/show/NCT014196915.
[13] https://clinicaltrials.gov/ct2/show/NCT01747798.
[14] C. Schmidt, A. Casini, *Organometallic Chemistry of Gold-Based Drugs, Comprehensive Organometallic Chemistry IV, Vol. 15*, Elsevier, Amsterdam, **2022**, pp. 297–313.
[15] D. Mustacich, G. Powis, *Biochem. J.* **2000**, *346*, 1–8.
[16] H. R. Shahsavari, N. Gimenez, E. Lalinde, M. T. Moreno, M. Fereidoonnezhad, R. B. Aghakhanpour, M. Khatami, F. Kalantari, Z. Jamshidi, M. Mohammadpour, *Eur. J. Inorg. Chem.* **2019**, 1360–1373.
[17] M. Serratrice, L. Maiore, A. Zucca, S. Stoccoro, I. Landini, E. Mini, L. Massai, G. Ferraro, A. Merlino, L. Messori, M. A. Cinellu, *Dalton Trans.* **2016**, *45*, 579–590.
[18] A. van Niekerk, P. Chellan, S. F. Mapolie, *Eur. J. Inorg. Chem.* **2019**, 3432–3455.
[19] a) J. Karges, T. Yempala, M. Tharaud, D. Gibson, G. Gasser, *Angew. Chem. Int. Ed.* **2020**, *59*, 7069–7075; *Angew. Chem.* **2020**, *132*, 7135–7141; b) A. Jain, *Coord. Chem. Rev.* **2019**, *401*, 213067.
[20] C. Schmidt, B. Karge, R. Misgeld, A. Prokop, R. Franke, M. Bronstrup, I. Ott, *Chem. Eur. J.* **2017**, *23*, 1869–1880.
[21] E. Wexselblatt, D. Gibson, *J. Inorg. Biochem.* **2012**, *117*, 220–229.
[22] J. Z. Zhang, E. Wexselblatt, T. W. Hambley, D. Gibson, *Chem. Commun.* **2012**, *48*, 847–849.
[23] S. Yuan, Y. Zhu, Y. Dai, Y. Wang, D. Jin, M. Liu, L. Tang, F. Arnesano, G. Natile, Y. Liu, *Angew. Chem. Int. Ed.* **2022**, *61*, e202114250; *Angew. Chem.* **2022**, *134*, e202114250.
[24] R. Raveendran, J. P. Braude, E. Wexselblatt, V. Novohradsky, O. Stuchlikova, V. Brabec, V. Gandin, D. Gibson, *Chem. Sci.* **2016**, *7*, 2381–2391.
[25] S. E. Eriksson, S. Prast-Nielsen, E. Flaberg, L. Szekely, E. S. Arner, *Free Radical Biol. Med.* **2009**, *47*, 1661–1671.
[26] E. S. Arner, A. Holmgren, *Curr. Protoc. Toxicol.* **2001**, Chapter 7, Unit 7.4.
[27] a) A. Pratesi, C. Gabbiani, E. Michelucci, M. Ginanneschi, A. M. Papini, R. Rubbiani, I. Ott, L. Messori, *J. Inorg. Biochem.* **2014**, *136*, 161–169; b) R. Rubbiani, I. Kitanovic, H. Alborzinia, S. Can, A. Kitanovic, L. A. Onambele, M. Stefanopoulou, Y. Geldmacher, W. S. Sheldrick, G. Wolber, A. Prokop, S. Wölfl, I. Ott, *J. Med. Chem.* **2010**, *53*, 8608–8618; c) P. Holenya, S. Can, R. Rubbiani, H. Alborzinia, A. Junger, X. Cheng, I. Ott, S. Wölfl, *Metallomics* **2014**, *6*, 1591–1601; d) R. Rubbiani, E. Schuh, A. Meyer, J. Lemke, J. Wimberg, N. Metzler-Nolte, F. Meyer, F. Mohr, I. Ott, *MedChemComm* **2013**, *4*, 942–948.
[28] a) X. Cheng, P. Holenya, S. Can, H. Alborzinia, R. Rubbiani, I. Ott, S. Wölfl, *Mol. Cancer* **2014**, *13*, 221; b) Y. Dabiri, M. A. Abu El Maaty, H. Y. Chan, J. Wölker, I. Ott, S. Wölfl, X. Cheng, *Front. Oncol.* **2019**, *9*, 438.
[29] A. Pratesi, C. Gabbiani, M. Ginanneschi, L. Messori, *Chem. Commun.* **2010**, *46*, 7001–7003.
[30] C. Gabbiani, G. Mastrobuoni, F. Sorrentino, B. Dani, M. P. Rigobello, A. Bindoli, M. A. Cinellu, G. Pieraccini, L. Messori, A. Casini, *MedChemComm* **2011**, *2*, 50–54.
[31] a) T. Agalioti, A. D. Giannou, A. C. Krontira, N. I. Kanellakis, D. Kati, M. Vreka, M. Pepe, M. Spella, I. Lilis, D. E. Zazara, E. Nikolouli, N. Spiropoulou, A. Papadakis, K. Papadia, A. Voulgaridis, V. Harokopos, P. Stamou, S. Meiners, O. Eickelberg, L. A. Snyder, S. G. Antimisiaris, D. Kardamakis, I. Psallidas, A. Marazioti, G. T. Stathopoulos, *Nat. Commun.* **2017**, *8*, 15205; b) Z. B. Jiang, W. J. Wang, C. Xu, Y. J. Xie, X. R. Wang, Y. Z. Zhang, J. M. Huang, M. Huang, C. Xie, P. Liu, X. X. Fan, Y. P. Ma, P. Y. Yan, L. Liu, X. J. Yao, Q. B. Wu, E. Lai-Han Leung, *Cancer Lett.* **2021**, *515*, 36–48.
[32] R. D. Starke, F. Ferraro, K. E. Paschalaki, N. H. Dryden, T. A. McKinnon, R. E. Sutton, E. M. Payne, D. O. Haskard, A. D. Hughes, D. F. Cutler, M. A. Laffan, A. M. Randi, *Blood* **2011**, *117*, 1071–1080.
[33] K. R. McSweeney, L. K. Gadanec, T. Qaradakhi, B. A. Ali, A. Zulli, V. Apostolopoulos, *Cancers* **2021**, *13*, 1572.
[34] a) E. Cheriathundam, A. P. Alvares, *J. Biochem. Toxicol.* **1996**, *11*, 175–181; b) Y. Yamanishi, M. Takeda, N. Honjo, K. Aoi, Y. Ishibe, S. Yamana, *Ryumachi* **1992**, *32*, 475–482.

Manuscript received: November 30, 2022
Accepted manuscript online: January 10, 2023
Version of record online: January 31, 2023